An instrument viewing the ocean from a satellite or aircraft measures upwelling radiances that include contributions by the atmosphere, the water surface, and the water column. The atmospheric contribution L_a comes from solar radiance that is scattered one or more times by atmospheric gases and aerosols into the direction of the sensor. The surface-reflected radiance (sun and sky glint) L_r is downwelling solar radiance that is reflected toward the sensor by the water surface. The water-leaving radiance L_w comes from light that is transmitted through the surface into the ocean, L_t, where it is changed by the absorbing and scattering components in the water, and is then scattered into an upward direction, L_u, and eventually leaves the sea surface in the sensor direction. Figure 1 shows this conceptually.

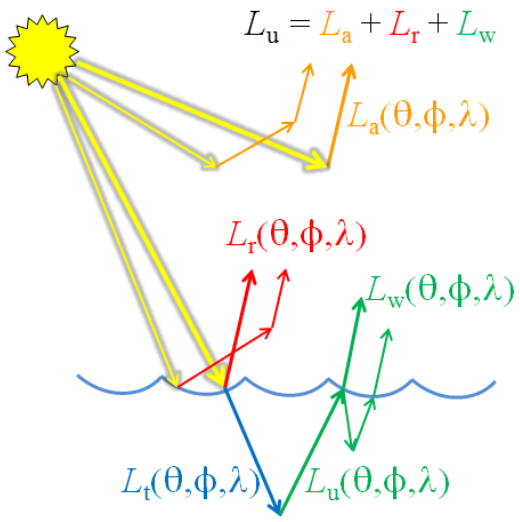

Figure 1: Fig. 1. Contributions to the total upwelling radiance above the sea surface, L_u. Yellow arrows are the sun's unscattered beam; orange arrows are atmospheric path radiance L_a; red is surface-reflected radiance L_r; green is water-leaving radiance L_w. Thick arrows represent single-scattering contributions; thin arrows illustrate multiple scattering contributions.

Radiance reflected by the sea surface contains information about the wave state of the surface, which may be of interest in itself or which, for example, may be useful for detection of surface oil slicks. Radiance scattered by the atmosphere along the path between the sea surface and the sensor contains information about atmospheric aerosols and other atmospheric parameters. However, only the water-leaving radiance carries information about the water column and bottom conditions. A sensor looking downward measures the total radiance $L_u = L_a + L_r + L_w$ and cannot separate the various contributions to the total. *Atmospheric correction* refers to the process of removing the contributions by surface glint and atmospheric scattering from the measured total to obtain the water-leaving radiance.

This page uses numerical atmosphere-ocean radiative transfer simulations to show examples of the nature and magnitude of the atmospheric correction problem. These figures were generated by a coupled MODTRAN-HydroLight radiative transfer code. The MODTRAN atmospheric code was used to propagate sunlight from the top of the atmosphere to the sea surface. The atmospheric radiance incident onto the sea surface was then used to initialize the HydroLight in-water code. HydroLight transmitted the radiance through the sea surface, computed its interaction with the water constituents, and eventually returned the water-leaving radiance back to MODTRAN. MODTRAN then propagated the water-leaving radiance, plus the glint radiance and atmospheric

path radiance, to the sensor. Both of these codes are for unpolarized radiance calculations.

Figure 2 shows examples of at-sensor total radiances L_u for different sensor altitudes. The inputs to MODTRAN were for

- cloudless mid-latitude summer atmosphere
- marine aerosols
- relative humidity of 76% at sea level
- solar zenith angle of 50 deg
- surface wind speed of 6 m s^{-1}
- nadir-viewing sensor

These atmospheric conditions gave excellent remote-sensing conditions with a horizontal visibility of 63 km at sea level. The HydroLight inputs were for

- homogeneous water
- Case 1 water with a chlorophyll concentration of 1 mg m^{-3}
- infinitely deep water

The runs were from 300 to 1000 nm with 10 nm bandwidths. The sun and viewing geometry gives almost no sun glint radiance. However, there is always surface-reflected sky radiance, which shows up in the surface (zero altitude) spectrum (black curve) as non-zero L_u radiance beyond 750 nm, where the water-leaving radiance is very close to zero. The differences in these curves are due solely to atmospheric contributions along the different path lengths from the sea surface to the sensor because all other conditions were the same for each curve. This figure shows that there is a noticeable atmospheric contribution to the total radiance even for sensors just a few hundred meters above the surface in very clear atmospheres. Airborne sensors typically fly at altitudes from 3,000 to 10,000 m, and even at lower altitudes the atmospheric contribution is greater than the water-leaving radiance. At 30,000 m, a sensor is effectively above the top of the atmosphere (TOA) and atmospheric path radiance is typically 90-95% of the total.

Figure 3 shows the Fig. 2 at-sensor radiance at 3,000 m partitioned into the contributions by water-leaving, surface-reflected, and atmospheric path radiances; the individual contributions can be separated in the numerical models. This altitude is typical for aircraft acquiring high spatial resolution hyperspectral imagery.

The atmospheric correction problem becomes even more intimidating when effects of sun and sensor viewing directions, atmospheric conditions, and surface wave state are considered. The following figures show a few examples of simulations performed in support of the design of the proposed NASA HyspIRI (Hyperspectral InfraRed Imager) mission. That sensor will measure radiances at the top of the atmosphere at 10 nm resolution from 380 to 2500 nm with 60 m ground resolution. The simulations shown below all have a chlorophyll value of 0.05 mg m^{-3} characteristic of the very clear Case 1 ocean water near the Hawaiian Islands. The atmospheric conditions are for either a very clear tropical atmosphere (horizontal visibility of 100 km at sea level) or one with considerable haze (horizontal visibility of 10 km). The wind speed was 0 (a level sea surface) or 10 m s^{-1}. The sensor viewing direction was 30 deg east of nadir, nadir, or 30 deg west of nadir.

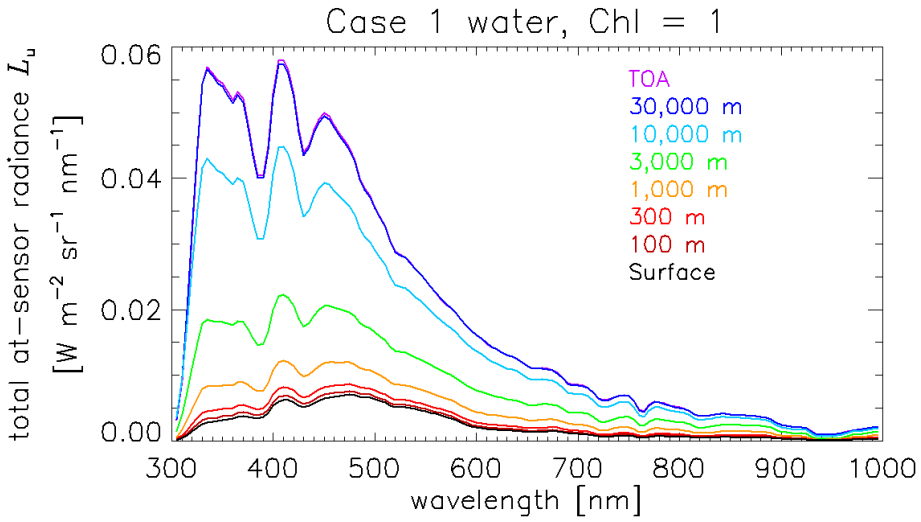

Figure 2: Fig. 2. Example at-sensor radiances L_u for different sensor altitudes. The water-leaving radiance and surface-reflected radiance (not shown) are the same in all cases.

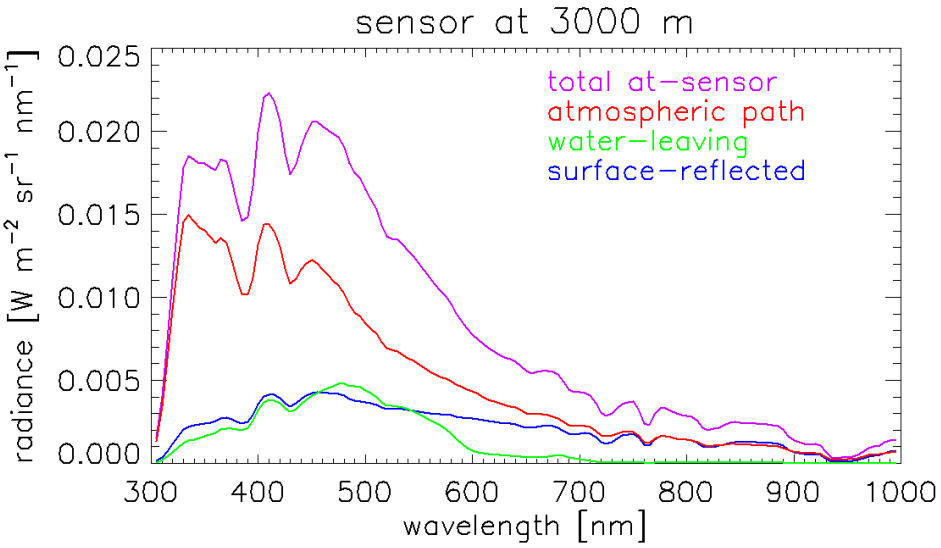

Figure 3: Fig. 3. The total radiance curve of Fig. 2 at 3000 m sensor altitude partitioned into the contributions by water-leaving radiance, surface reflectance, and atmospheric path radiance.

The sun zenith angle was 18 deg, which corresponds to the time of the satellite overpass on 21 June at Station Aloha, near Hawaii.

Figure 4 shows the TOA radiances computed for the clear atmosphere, wind speed of U = 10 m s^{-1}, and a viewing direction of 30 deg east of the satellite nadir direction. The blue curves are the total radiance L_u, orange is atmospheric path radiance L_a, green is water-leaving radiance L_w, and red is sun and sky glint L_g. The solid lines are the radiances measured at the TOA and the dashed lines are radiances at the sea surface. Thus the dashed green curve is the true water-leaving radiance just above the sea surface. The solid green curve is how much of L_w at the surface makes it to the TOA; the rest is lost to absorption and scattering along the path from the sea surface to the TOA. The TOA L_u curve is the sum of the TOA atmospheric, water-leaving, and glint radiances. The surface (SFC) L_u curve is the sum of the corresponding surface contributions; note that there is no atmospheric contribution at the surface. The atmospheric correction problem is to measure the solid blue spectrum and then extract the dashed green spectrum.

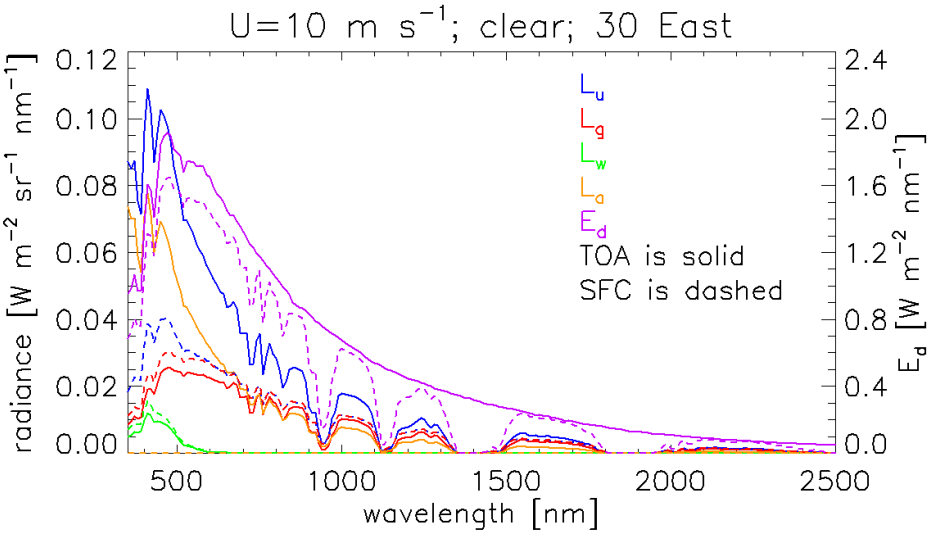

Figure 4: Fig. 4. Radiances and irradiances for a clear atmosphere, wind speed of 10 m s^{-1}, viewing direction 30 deg east of nadir. Solid lines are values at the top of the atmosphere (TOA); dashed lines are at the sea surface (SFC).

Figure 4 also shows the plane irradiance E_d at the TOA and sea surface. Water-vapor and CO_2 absorption bands centered near 1400 and 1900 nm reduce the sea-level E_d to essentially zero in those spectral regions.

Most remote-sensing retrieval algorithms use the remote-sensing reflectance $R_{\rm rs} = L_w/E_d$ or an equivalent nondimensional reflectance $\rho = \pi L_w/E_d$. (If L_w were directionally isotropic, $R_{\rm rs} = 1/\pi$, so ρ is the ratio of the actual $R_{\rm rs}$ to an idealized isotropic remote-sensing reflectance. The π carries units of steradian.) The use of an apparent optical property like $R_{\rm rs}$ or ρ minimizes the effects of external environmental conditions like sun angle on the magnitude of the spectra.

Figure 5 plots the same information as Fig. 4 but in terms of ρ. The TOA ρ spectra were computed from the TOA radiances divided by the TOA E_d; the surface ρ spectra were computed from surface radiances divided by the surface E_d. The surface sun and sky glint ρ_g spectrum was not plotted near 1900 nm because the E_d values at the sea surface were too small for accurate numerical computation (a small effect of numerical inaccuracy in ρ_g(SFC) is also seen near 1350 nm). Note that the surface glint reflectance spectrum ρ_g (red dashed curve) is nearly independent

of wavelength because the glint radiance spectrum has almost the same wavelength dependence as the surface irradiance that is being reflected by the sea surface.

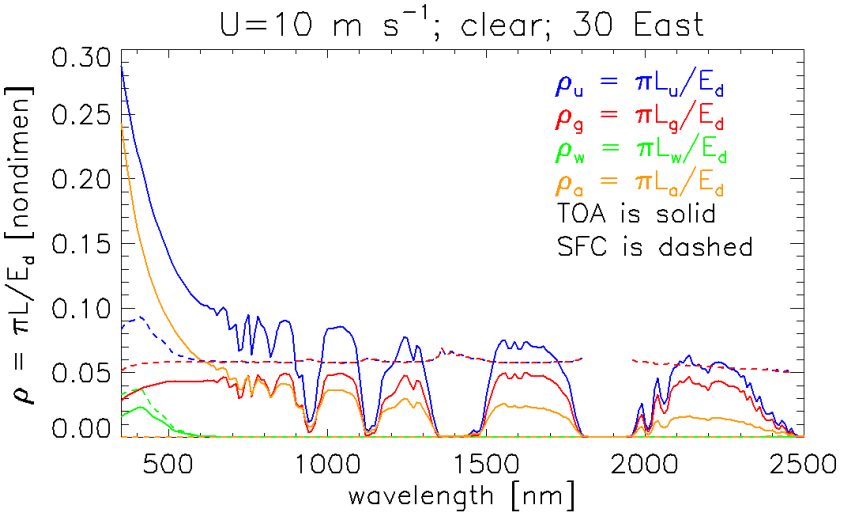

Figure 5: Fig. 5. The same information as in Fig. 4, but plotted as nondimensional reflectances ρ.

Figure 6 compares the ρ spectra for viewing directions of 30 deg east of nadir, nadir, and 30 deg west of nadir. The sky was clear and the wind speed was 10 m s^{-1}. The ρ_g spectra are much different for the different viewing directions. The sun is almost due east and high in the sky, so the 30 deg east viewing direction sees a lot of sun glint and has a high-magnitude ρ_g. The 30 deg west viewing direction sees very little sun glint and has a ρ_g that is mostly sky reflectance. The atmospheric path radiances are noticeably different for the three viewing directions because of the different scattering angles between the sun's direct beam and the viewing direction, and because of the differences in path length through the atmosphere for the east and west vs nadir directions. The water-leaving reflectances ρ_w are almost independent of viewing direction. The almost unnoticeable (in this figure) differences in the three ρ_w curves are due to differences in the in-water scattering angles and path lengths.

Figure 7 shows the ρ spectra for clear vs. hazy sky conditions. The wind speed was 10 m s^{-1} and the viewing direction was 30 deg west. The differences in atmospheric path radiance are most pronounced in the infrared. There is some difference in the surface glint spectra because the glint for the hazy atmosphere contains more sky reflectance and less direct sun glint than for the clear sky case. The water-leaving radiances are indistinguishable in the plot.

Figure 8 shows the effect of wind speed for a clear sky and a nadir viewing direction. The large difference in the surface reflectance spectra ρ_g is due to the large amount of direct sun glint in the 10 m s^{-1} case. There is only sky glint when the surface is level. The atmospheric path reflectances are different because the different wind speeds result in different concentrations of aerosols in the marine boundary layer.

Figure 9 summarizes Figs. 5-8 by showing the 12 ρ_u spectra at the TOA for the two winds speeds of 0 and 10 m s^{-1}, the two sky conditions of clear and hazy, and the three viewing directions of 30 deg east, nadir, and 30 deg west. As before, the green spectrum at the bottom is ρ_w, which is almost the same for each of the 12 ρ_u spectra. Given any of the ρ_u spectra measured at the TOA, one must some way extract the surface ρ_w spectrum. This is clearly a difficult task owing to the non-unique relation between TOA and water-leaving radiances, and it is only partially solved.

Atmospheric correction is the central problem of ocean color remote sensing. However, the

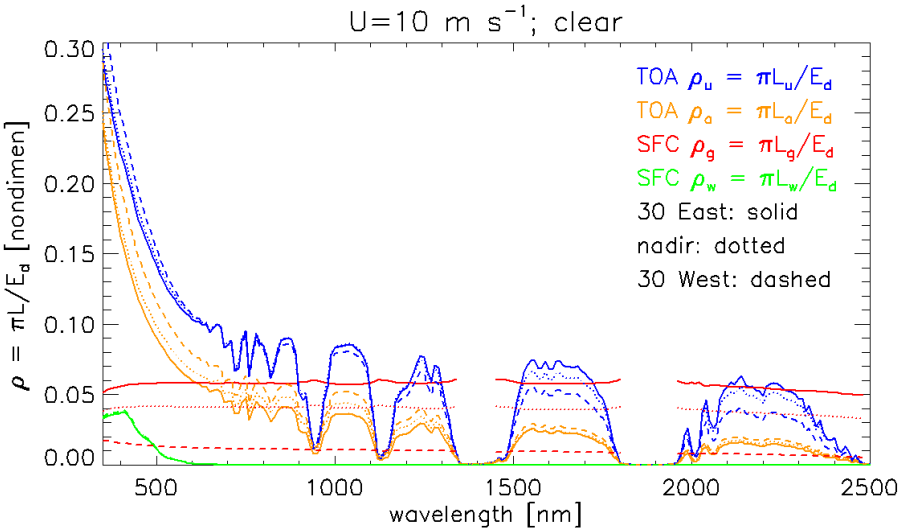

Figure 6: Fig. 6. Comparison of sensor viewing directions for a 10 m s^{-1} wind speed and a clear sky.

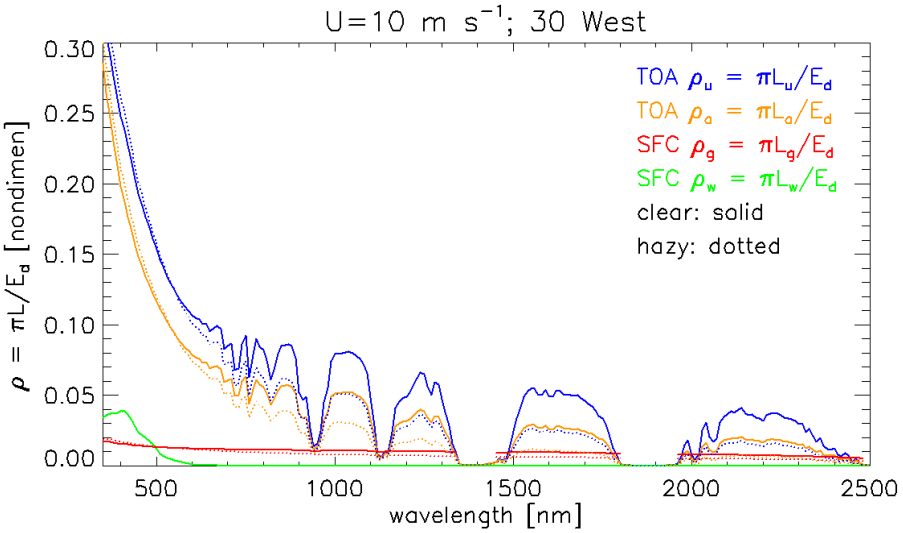

Figure 7: Fig. 7. Comparison of clear vs. hazy atmospheric conditions for a wind speed of 10 m s^{-1} and a viewing direction of 30 deg west of nadir.

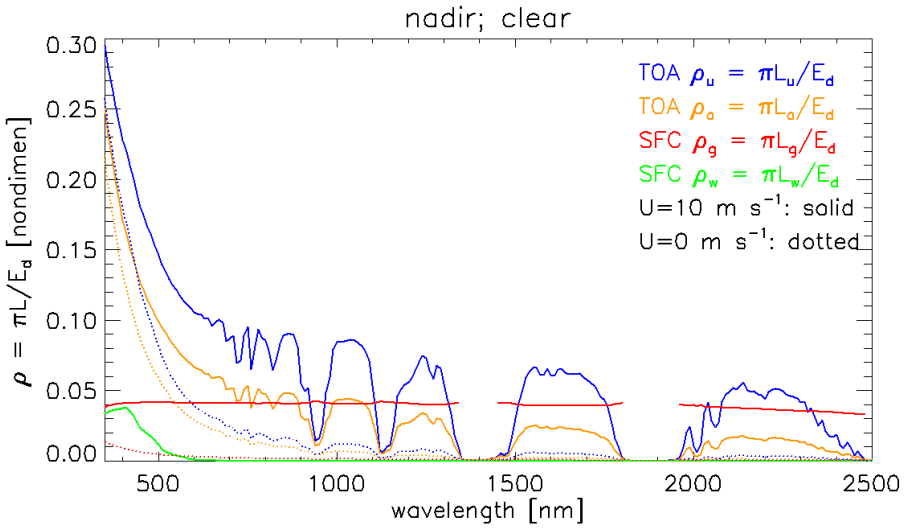

Figure 8: Fig. 8. Comparison of wind speeds for a nadir viewing direction and a clear sky.

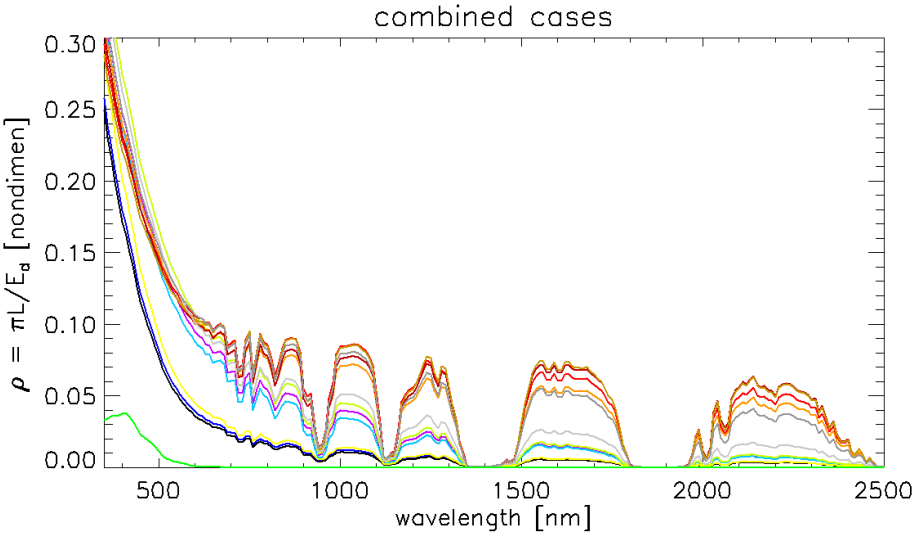

Figure 9: Fig. 9. The 12 ρ_u(TOA) spectra of Figs. 5-8. Each one has the almost the same water-leaving reflectance spectrum (bottom green curve).

problem is not intractable–if it were, we could not do ocean color remote sensing! There are many inversion algorithms that can retrieve ocean properties such as chlorophyll, mineral, or CDOM concentrations, or bottom depth and reflectance, IF an accurate ρ_w is available. The hard part of the game is to get from ρ_u measured at the TOA to ρ_w at the sea surface. The process of atmospheric correction is considered in detail in the Atmospheric Correction chapter.